Microspectroscopic Analysis of the X-Ray-induced Photoreduction in Fe- and Mn-containing SMMs

Norman Schmidt[a], Andreas Scheurer[b], Stefan Sperner[b], and Rainer H. Fink[a]

[a] Department Chemie und Pharmazie, Physikalische Chemie II und ICMM, Universität Erlangen-Nürnberg, Egerlandstraße 3, 91058 Erlangen, Germany
[b] Department Chemie und Pharmazie, Lehrstuhl für Anorganische und Allgemeine Chemie, Universität Erlangen-Nürnberg, Egerlandstraße 1, 91058 Erlangen, Germany

Reprint requests to Prof. Dr. R. Fink. Fax: (+49) 9131-85-28867.
E-mail: rainer.fink@chemie.uni-erlangen.de

Z. Naturforsch. **2010**, *65b,* 390 – 398; received December 23, 2009

Dedicated to Professor Rolf W. Saalfrank on the occasion of his 70th birthday

Scanning transmission X-ray microspectroscopy (STXM) and L-edge near-edge X-ray absorption fine structure (NEXAFS) spectroscopy have been applied to study the valence states of metal ions in various Fe- and Mn-containing single-molecule magnet materials, in particular the ligand-stabilized metal complexes $NaFe_6$ (so-called "ferric wheel"), Fe_4 (so-called "ferric star") and Mn_7 (so-called "manganese wheel"). We compare dose-dependent L-edge absorption spectra with the results of theoretical studies of the involved metal ions to conclude on the change in oxidation state upon increasing the X-ray dose. It is found that even low-intensity irradiation induces the reduction of the weakly interacting metal ions, and that the soft X-ray-induced photoreduction is less pronounced in microcrystalline films.

Key words: Single-molecule Magnet (SMM), X-Ray Absorption, X-Ray Microspectroscopy, STXM, Photoreduction

Introduction

The achievements in supramolecular coordination chemistry [1 – 4] enabled a fast development in the field of molecular magnetism [5] during the last 15 years. Substances which show the typical single-molecule magnet (SMM) [6] behaviour are mostly polynuclear transition metal complexes. At very low temperatures, they behave like classical ferromagnets and show magnetic bistability [7] (*i. e.* a memory effect) and ferromagnetic hysteresis [8]. In addition, these supramolecular compounds show the very interesting phenomenon of quantum tunnelling of magnetization [9]. The driving force behind these effects is the coupling of spins of each individual metal ion within one molecule, thus representing a molecular nanomagnet. The most prominent representative in this context is Mn_{12} [10], a supramolecule containing four Mn^{4+} and eight Mn^{3+} ions, which are connected by μ_3-oxo and μ_2-acetato ligands, and a number of derivatives of this compound. The second prominent SMM is the octanuclear complex Fe_8 [11], its Fe^{3+} ions being connected by μ_2-hydroxo and μ_3-oxo ligands and stabilized by triazacyclononane (tacn) ligands. Families of complexes with smaller cores like Mn_7 [12, 13], Mn_4 [14] or Fe_4 also exist. The four Fe^{3+} ions in Fe_4 are arranged in the form of a planar three-spiked star. In one case the ions are connected by μ_2-methoxy ligands and saturated by dipivaloylmethane (dpm) [15], and in another case deprotonated diethanolamine is acting both as a μ_2- and μ_3-O bridging and a coordination-saturating ligand [16]. The various substances are considered to be interesting candidates for data storage [17] (with faster access and higher density than conventional magnetic data storage devices), for application as contrast agents in magnetic resonance imaging [18, 19], in quantum computers [17, 20, 21] and in the modern field of spintronics [22, 23].

Besides the magnetic behaviour, which has been addressed in many reviews [24 – 28], the chemical properties are important since the valence states of the ions in the multinuclear complexes govern the overall magnetic properties whereas the stabilizing ligands affect the intramolecular magnetic coupling. Recent scan-

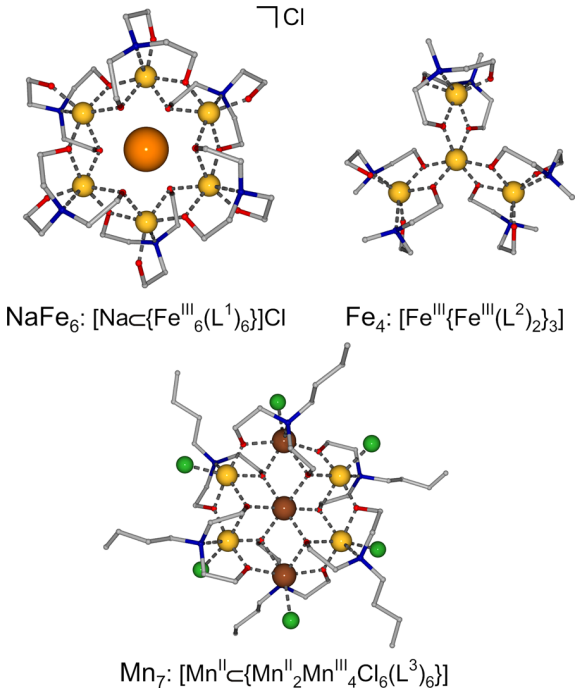

Fig. 1. Molecular structure of the ferric wheel $NaFe_6$ (top left; H_3L^1 = triethanolamine), the ferric star Fe_4 (top right; H_2L^2 = *N*-methyldiethanolamine), and the mixed-valent manganese wheel Mn_7 (right; H_2L^3 = *N*-*n*-butyldiethanolamine) [hydrogen atoms, disorder, and non-coordinating solvent molecules omitted for clarity; Fe^{III}/Mn^{III} gold, Na^I orange, Mn^{II} brown, Cl green, O red, N blue, C gray (colour online)].

ning tunnelling spectroscopy (STS) studies have monitored the individual metal centers within these ligand-stabilized complexes [16, 29].

Various electron spectroscopies have been successfully applied to study valence states. Combined studies using X-ray photoelectron spectroscopy (XPS), X-ray absorption and X-ray emission have been used to investigate, *e. g.*, Mn_{12} and derivatives [30 – 33], together with Fe_8 [30] and Fe_4 [34], in some cases supported by DFT studies [30, 31, 34]. X-Ray absorption spectroscopy is the basic technique to access the spin and orbital moments separately in X-ray circular magnetic dichroism (XMCD) spectroscopy, which has been employed for Mn_{12} [35, 36], Fe_8 [35], a Fe_4 derivative [37, 38], and several other SMMs [39, 40]. Some recent experiments [33], however, have demonstrated that the application of brilliant synchrotron radiation affects the spectral signatures. These X-ray absorption studies of various Mn_{12} derivatives clearly indicate that, even in monolayers, intense radiation induces a photoreduction of these single molecule magnets containing manganese. This may be attributed to the insufficient intramolecular shielding of the core-hole excitation in the weakly bound molecules.

In the present study, we report on the X-ray absorption study of various SMMs, in particular $NaFe_6$ [41], Fe_4 [42], and Mn_7 [13] (see Fig. 1). In a strict sense, the investigated iron coronate $NaFe_6$ is not a single-molecule magnet, but an antiferromagnetically coupled ring, and therefore has a ground state total spin of $S = 0$ at zero field. Nonetheless, it has interesting magnetic properties and shows a hysteresis loop [43]. Fe_4 contains four Fe^{3+} ions and has a ground state total spin of $S = 10/2$ due to the antiferromagnetic coupling of the three peripheral ions to the central ion. Its SMM behaviour has been intensely studied [16, 29, 34]. Other groups have studied similar molecules with a Fe_4 core but different ligands [38]. In Mn_7, four Mn^{3+} ions (two pairs) with two Mn^{2+} ions in between are arranged in a six-membered ring, which is centered by another Mn^{2+} ion. Like in Fe_4, the different manganese ions are bridged by μ_2- and additionally μ_3-O functions of the tridentate diethanolamine ligand, with the coordination sphere being saturated by chloride. The intramolecular coupling is mostly ferromagnetic, resulting in a ground state total spin of $S = 27/2$ at zero field [13].

We used scanning transmission X-ray microspectroscopy (STXM) and conventional NEXAFS spectroscopy to record the NEXAFS spectra of the substances mentioned above. STXM offers a direct comparison of the electron spectroscopy signature with the morphology of condensed SMMs. In addition, very short illumination times in STXM offer a tool to study the effect of X-ray illumination in more detail. The interpretation of the spectra with respect to the oxidation state of the metal ions is mainly based on calculated multiplet spectra and to some extent on the comparison with various related compounds. It will be demonstrated that these polynuclear transition metal complexes are extremely sensitive to soft X-ray illumination and that radiation-induced reduction of the metal ions has to be considered in all cases.

Experimental Details

The STXM experiments were performed at the Environmental STXM (undulator beamline BL 11.0.2) at the Advanced Light Source (ALS, Berkeley, USA) [44]. The sample is raster-scanned across the focal spot of a Fresnel zone plate, thus offering 2D projections of ultrathin samples with lateral

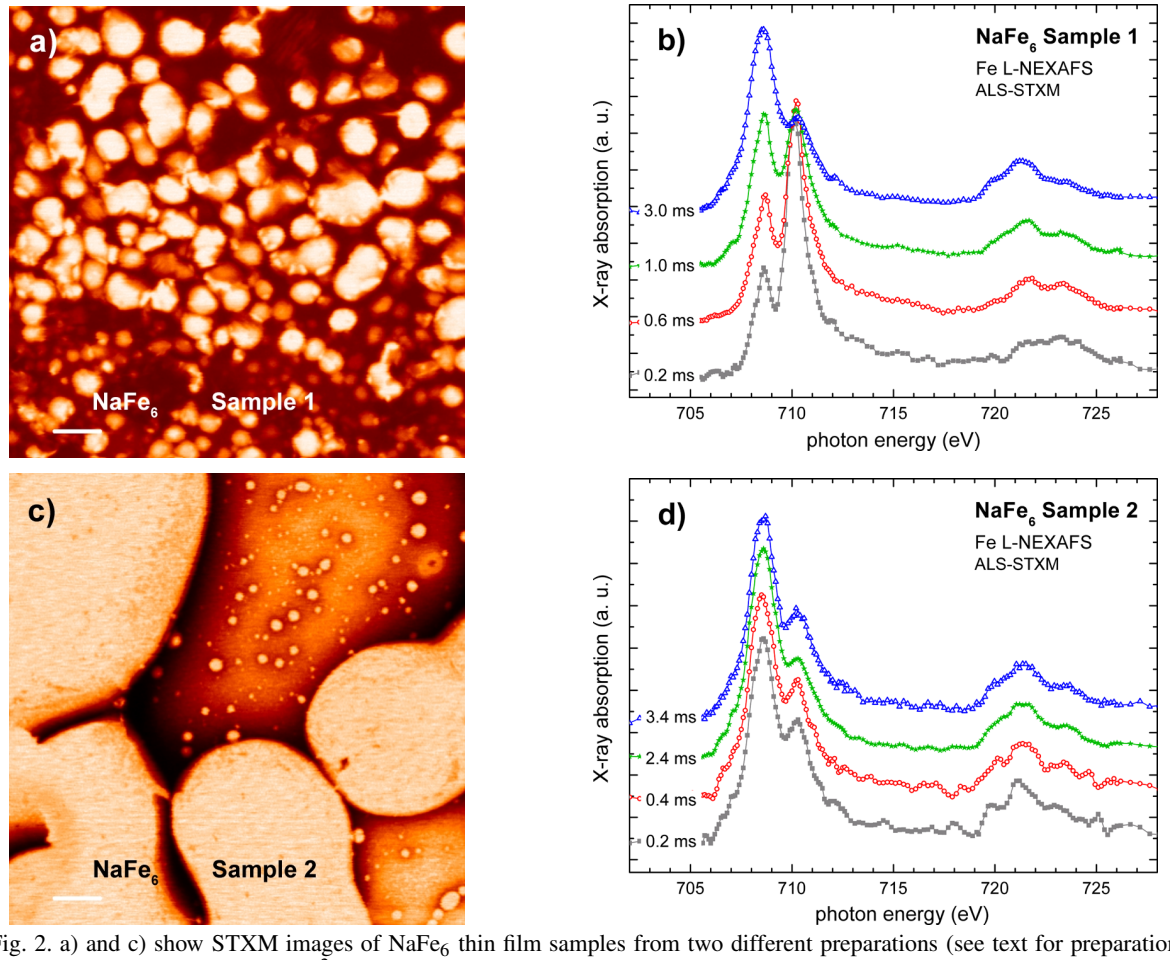

Fig. 2. a) and c) show STXM images of $NaFe_6$ thin film samples from two different preparations (see text for preparation details; image sizes: 20 × 20 μm^2, photon energy: 708.4 eV, dwell times: 0.3 ms); b) and d) show the corresponding Fe L-edge NEXAFS spectra as derived from STXM line scans using the indicated integral dwell times, *i. e.* illumination per spot during the energy scans (colour online).

resolutions in the range of several 10 nanometers, thereby providing direct access to the sample morphology. The Fe and Mn L-edge absorption spectra were derived from line scans using different dwell times per pixel (from 100 μs to several ms). The samples were recorded in He atmosphere at r. t., and no magnetic fields were applied. The energy calibration has an accuracy of 0.3 eV.

Standard NEXAFS experiments were performed at the UE-52 undulator beam line at the BESSY II storage ring (Berlin, Germany). The beamline provides a flux of 3 × 10^{11} photons/(s × 100 mA) with a typical energy resolution of about 100 meV for Fe and Mn 2*p* absorption spectra. At the time of the measurements, the storage ring operated in single bunch mode with a beam current of 10 – 15 mA, thus providing a 20 times lower photon flux than in normal mode and a slightly bigger spot size. The NEXAFS data were recorded in partial electron yield mode using retarding voltages of 150 V. The recording time for one single spectrum was around 10 min. The measurements were performed at r. t. and with a 55° angle of incidence of the synchrotron radiation. The spot size of the synchrotron light is around 1 mm^2, thus averaging over a large sample area. The spectra were only corrected for ring current, since the I_0 spectrum in the Mn 2*p* and Fe 2*p* regions is essentially flat. Energy calibration was done by XPS measurements of a clean gold foil with the excitation energy of the most important resonance in the respective NEXAFS spectra. The experimental end station consists of a load-lock, a preparation chamber and an analysis chamber operating at a base pressure in the 10^{-10} mbar regime.

The synthesis of $NaFe_6$ [41], Fe_4 [42] and Mn_7 [13] has been described elsewhere. The investigated samples were

prepared *ex-situ* by dissolving the different complexes in high-purity chloroform and subsequently dropping the solution onto pristine or gold-plated Si(100) wafer pieces. After evaporation of the solvent, this preparation resulted in films of inhomogeneous microcrystalline conglomerates. The samples were mounted to a sample holder with conductive double-faced adhesive tape, introduced into the loadlock and outgassed for several hours under ultrahigh vacuum conditions.

In addition to the experimental study, we used the CTM4XAS software to simulate the Mn 2*p* and Fe 2*p* X-ray absorption spectra [45]. In the calculations we assumed an octahedral ligand sphere with a splitting of 10 dQ = 1.5 eV in the initial and final states for all relevant ions. Lorentzian and Gaussian broadening was both set to 0.3 eV. The resulting spectra are conclusive enough with respect to the determination of the oxidation state, therefore a more exact treatment of the ligand sphere can be neglected.

Experimental Results and Discussion

NEXAFS studies of $NaFe_6$

Fig. 2 compares Fe L-edge spectra from two differently prepared $NaFe_6$ samples, which show differences in film morphology due to different preparation procedures. Scanning transmission X-ray micrographs (image size 20 × 20 μm^2) recorded at a photon energy of 708.4 eV reveal different thickness variations for the two investigated samples. For sample 1 (Fig. 2a), the solvent was quickly removed, thus leading to a microcrystalline morphology, whereas for slow solvent removal a more homogeneous film could be prepared (sample 2, Fig. 2c). The bright areas in Fig. 2c correspond to regions where the film did not wet the Si_3N_4 substrate. From better resolved images we can exclude the formation of nanocrystalline structures.

Fe L-edge NEXAFS spectra were extracted for both $NaFe_6$ samples from subsequent line scans. Fig. 2b compares the NEXAFS spectra for sample 1 for increasing dwell times from bottom to top. The most obvious changes are observed at the L_3 edge (photon energy range from 707 to 712 eV). With increasing illumination times the intensity of the resonance at 708.5 eV increases at the expense of the higher energy resonance at 710 eV. These two resonances can be considered as a characteristic fingerprint for octahedrally coordinated Fe in the Fe^{3+} (710 eV) or Fe^{2+} state (see also below). At the L_2 edge the changes are not as clearly visible in the present spectra due to its lower intensity. This gradual change thus reflects the change in the valence state of the original Fe^{3+} state in $NaFe_6$. Astonishingly, the effect in sample 2 is very different. In this case, the intensity of the low-energy resonance dominates the spectra even for shortest dwell times, *i. e.* for 200 μs. We have to assume that imaging the film with dwell times as low as 0.3 ms prior to the spectroscopic investigations (see Fig. 2d) already induces chemical variations of the complex in this special film configuration. In the case of the polycrystalline arrangement in sample 1, much longer illumination times are acceptable prior to spectral changes.

NEXAFS investigations of Fe_4

The Fe_4 complex has previously been investigated by various research teams with respect to its electronic properties by X-ray absorption spectroscopy [34] and combined analysis of the electronic and magnetic properties of a similar Fe_4 derivative [38]. In the Fe_4 complex investigated herein, all metal ions are considered to be in a trivalent state. Fig. 3 compares the Fe L-edge NEXAFS spectra of microcrystalline Fe_4 as recorded subsequently at the BESSY UE52-PGM beamline. Compared to the spectra in Fig. 2, the overall signal-to-noise ratio is improved due to longer dwell times.

The first spectrum (Fig. 3, bottom) has a prominent L_3-edge resonance at 710.2 eV and a sharp spectral feature at 708.7 eV. In addition, there is a weak shoulder on the low-energy side of this resonance. In sub-

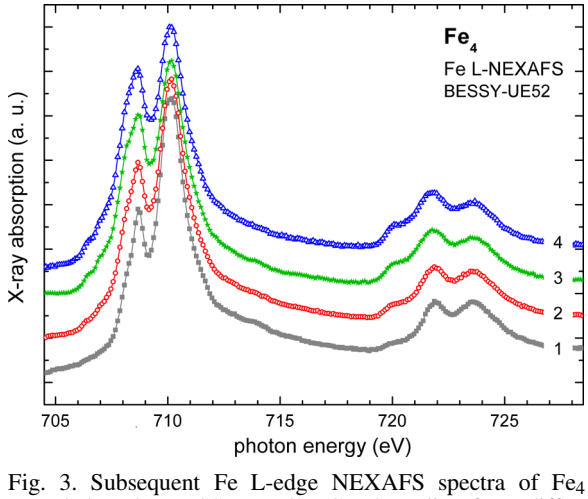

Fig. 3. Subsequent Fe L-edge NEXAFS spectra of Fe_4 recorded at the BESSY UE52-PGM beamline from different scans (1 – 4, dwell time per energy point: 1 s at significantly lower photon flux densities compared to STXM analysis) (colour online).

sequent spectra, the intensity of the prominent resonance decreases, whereas the low-energy resonance increases. In particular, the onset of the resonance gets more pronounced, and the previous clearly resolved feature at about 714 eV vanishes. Similar changes in intensity, *i. e.* the increase of the intensity of the low-energy features at the expense of the high-energy features are also observed in the L_2-edge region. The observed spectral changes, as in the case of polycrystalline $NaFe_6$, reflect a reduction from trivalent to divalent iron, owed to chemical changes upon increased soft X-ray irradiation. However, a complete transformation into a prominent low-energy feature at about 709 eV is not observed in the present study, most probably due to the fact that conventional NEXAFS uses much lower photon flux densities. There, spot sizes of about 1 mm are used compared to 150 – 200 nm in STXM (in the low-resolution mode as in our spectroscopic studies).

Comparison of the supramolecular Fe complexes

Fig. 4 compares the previously presented experimental spectra of $NaFe_6$ and Fe_4 with the theoretical spectra assuming Fe^{2+} and Fe^{3+} in an octahedrally coordinated site. The simplified calculations show that a change from Fe^{3+} to Fe^{2+} results in a shift in both the L_3 and L_2 edges of about 2.5 eV to lower energies together with some minor changes in relative intensities of the spectral features. Comparing the two Fe-containing complexes, we observe a similar trend in both cases. First, all iron ions have a similar chemical environment, which is reflected in very similar absorption properties, at least for the first recorded spectra. Second, upon increased irradiation with soft X-rays the intensity of the most prominent resonance around 710.5 eV is reduced. In the case of the ferric star, the low energy resonance increases to an almost similar intensity, whereas for $NaFe_6$ it exceeds the high-energy resonance by far. From the direct comparison with the theoretical spectra we may thus conclude that the spectral changes are mainly due to the change in the valence state of the involved Fe ions, *i. e.*, for higher doses the metal ions are photoreduced from Fe^{3+} to Fe^{2+}. We explain the incomplete chemical change in Fe_4 with significantly lower photon flux densities in conventional NEXAFS experiments compared to STXM microanalysis.

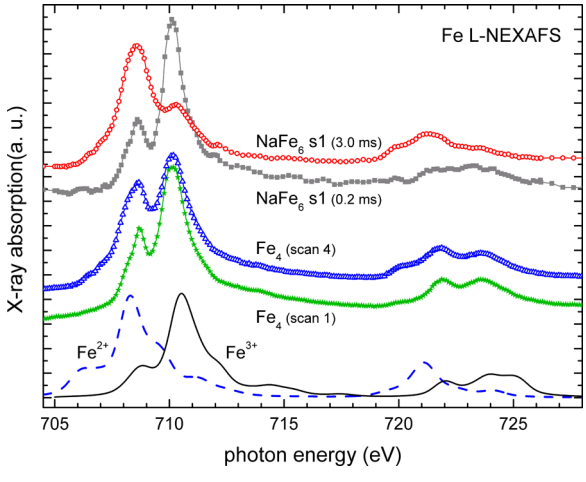

Fig. 4. Comparison of the experimental Fe L-edge NEXAFS spectra of $NaFe_6$ (sample 1, top two spectra, selected spectra from Fig. 2) and Fe_4 (center) with calculated NEXAFS spectra (bottom) for Fe^{2+} (dashed line) and Fe^{3+} (solid line) in octahedral coordination (colour online).

XAS data on Fe_4 have been published earlier by Takács *et al.* [34] and for a different but analogous Fe_4 ferric star by Mannini *et al.* [38]. Our own low-dose spectra reproduce the latter very well, which confirms our interpretation concerning the valence states. The measurements by Takács *et al.*, however, show no recognizable intensity on the low-energy side of the main resonance and only one prominent resonance in the L_2 region, thus resembling more the spectral characteristics of octahedrally coordinated Fe^{2+} ions.

NEXAFS studies of Mn_7 complexes

X-Ray absorption spectra of Mn_7 are shown in Fig. 5. As in the case of $NaFe_6$, the spectra were extracted from subsequent STXM line scans using different dwell times to explore potential changes in the Mn valence state upon irradiation. For the interpretation of the Mn L-edge NEXAFS spectra we have to keep in mind that Mn_7 is a mixed-valent species and contains three Mn^{2+} ions together with four Mn^{3+} ions. The most pronounced changes in the series of spectra concern the resonance at 640.5 eV, which greatly increases in intensity with increasing radiation dose. The same is true for the shoulder at 639.5 eV and the low-energy resonance in the L_2 region at 650.5 eV, though to a smaller extent. On the other hand, the high-energy shoulder of the resonance at 641.8 eV diminishes greatly in intensity from the first to the second scan.

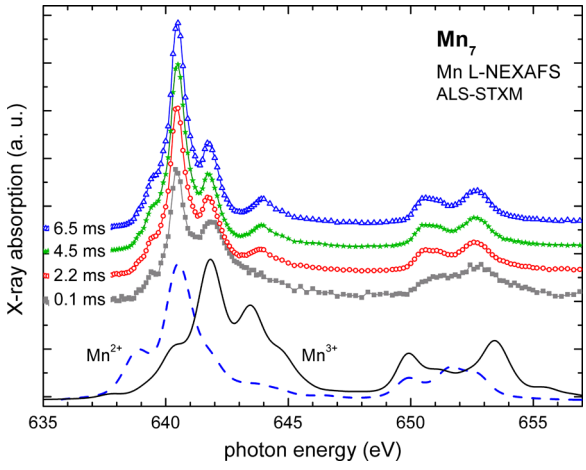

Fig. 5. Mn L-edge NEXAFS of Mn_7 derived from subsequent STXM line scans (integrated illumination time per data point is indicated for each spectrum) in comparison with calculated spectra of Mn^{2+} and Mn^{3+} in the corresponding coordination (colour online).

The relative intensities of the first two resonances change with increasing irradiation. It is very obvious that the major spectral changes occur from the first (0.1 ms) to the second scan (2.2 ms). The first spectrum was recorded with a dwell time of 100 μs (at slightly higher noise level), whereas for the subsequent spectra the dwell times were increased by at least a factor of 20. Thus, the irradiation dose during the second energy scan was already higher compared to the first spectrum even before the main absorption resonances were reached. After three subsequent spectra with a total dwell time of around 4.5 ms per measured data point, no noteworthy spectral changes were observed any more and a kind of saturation had been reached.

Comparing the measured and calculated spectra and also the experimental spectra of the single-valence manganese oxides Mn_2O_3 (Mn^{3+} only) and MnO (Mn^{2+} only) [32], the first (0.1 ms) spectrum can be interpreted as a stoichiometric mixture of Mn^{2+} and Mn^{3+} as expected for the intact molecule. With increasing irradiation dose, the spectra resemble more the calculated spectrum for Mn^{2+} in the L_3 region. In the L_2 region, the changes are much more subtle and cannot easily be explained by the calculations. However, neither from the spectral changes nor from the direct comparison with our theoretical data, we can quantify the degree of reduction upon irradiation. In many cases, the features of Mn L-edge spectra are affected by subtle structural modifications, and thus deconvolution of the spectra of mixed-valent compounds seems impossible [46, 47].

While for single crystals of Mn_{12} derivatives no spectral changes after irradiation for two hours at a low-flux beamline were reported [32], the authors found a significant Mn^{2+} contribution in XAS spectra of chemically bound monolayers of the same molecules on Au surfaces. This finding was attributed to a molecular decomposition by loss of ligands from the Mn_{12} cores. A later study by the same authors [33], where NEXAFS spectra of single crystals and monolayers of Mn_{12} derivatives from a low-flux and a high-flux bending magnet beamline were compared, has clearly shown that there is degradation due to any X-ray exposition, with a faster degradation of monolayers. A temperature-independent degradation of Mn_{12}-biph single crystals was found already after 2 min of irradiation at the PM3 bending magnet beamline, and after 15 min on the RGBL bending magnet beamline significant degradation of Mn_{12}-pfb single crystals was observed. In all cases, the spectra changed from a mixture of Mn^{3+} and Mn^{4+} to a mixture of Mn^{2+} and Mn^{3+}. This is in agreement with our findings on Mn_7, where the ratio of Mn^{2+} to Mn^{3+} in the complexes leans to Mn^{2+} upon prolonged X-ray irradiation.

Conclusions

In the present study we investigated three different SMMs which contain either iron or manganese in tri- or mixed-valent (II/III) oxidation states. Soft X-ray absorption fine structure spectroscopy was applied to monitor the electronic structure and the changes of the spectral features upon prolonged irradiation. The main spectral features were compared with the results of theoretical calculations where the respective di- and trivalent transition metal ions are octahedrally coordinated. The calculations did not include any kind of charge transfer and purely refer to the coordination of the metal ions and the involved multiplet splitting. In all cases, this simplified theoretical model allows one to qualitatively reproduce the experimental spectra quite well. From this comparison, we have been able to properly assign the spectral features to the respective oxidation states.

Mn_7, the Fe_4 ferric star and the polycrystalline sample of $NaFe_6$ exhibit pronounced changes in the valence state with ongoing irradiation, *i. e.*, the valence states change from +III to +II. For $NaFe_6$ it has been

demonstrated that the morphology obviously affects the degradation. We should note that we cannot exclude that the more homogeneous film of $NaFe_6$ (sample 2) experienced a reduction during film preparation or during microscopic imaging. Since STXM uses much higher photon flux densities compared to conventional soft X-ray absorption experiments, the chemical changes already occur on a much smaller time scale in STXM. This might explain why $NaFe_6$ is completely photoreduced even at very short exposures, whereas in Fe_4 the photoreduction has not yet reached saturation after several NEXAFS scans.

Several earlier publications have pointed to the effect of X-ray-induced photoreduction in XPS of $K_3(Fe,M)(CN)_6$ [48], the reduction of Ni^{4+} to Ni^{2+} [49] and of Fe^{3+} to Fe^{2+} [50] in complexes upon soft X-ray irradiation, and the reduction of iron and manganese ions in enzymatic cofactors [51 – 53] in X-ray crystallography (*i. e.*, hard X-rays). A more recent publication [54] summarizes this together with new data on X-ray photooxidation of low-valent and photoreduction of high-valent iron species and tries to quantify the effect. Photoreduction by soft X-rays (called SOXPR [49]) is found to be proportional to the photon flux or dose, but can occur in subsequent steps with different slopes, and also depends on the wavelength of the irradiation.

The SMMs investigated herein have similar structural features as some of the enzymatic cofactors for which structural data exist for their unreduced and photoreduced forms. In these cofactors, bridging μ_2-oxo ligands were found to be changed to non-bridging hydroxo or aquo ligands upon photoreduction (induced by hard X-rays) of Mn^{3+} [51, 52]. Since in proteins the metal ions are highly diluted and therefore seldomly excited directly, the likely primary process is the generation of free electrons in the sample (*e. g.*, photoelectrons, Auger electrons). These free electrons can be captured by the electrophilic high-valent metal ions which are thereby reduced. Additionally, photoexcitation can lead to homolytic bond cleavage within the ligands, creating a number of different radicals. H radicals can recombine with oxo ligands together with electron transfer to the metal ion, resulting in a hydroxo ligand bound to a reduced metal center. Other processes like a photon-induced electron transfer from a ligand to the metal center (LMCT) [55] also have to be considered.

In the case of the investigated SMM complexes, none of these processes can be excluded. In addition, we have to emphasize that our studies are not sufficient to favour any of the discussed processes. However, as has been shown for other organic systems, radiation-induced damage effects are less severe if organic molecules are sufficiently strongly coupled to electron reservoirs like in, *e. g.*, strongly interacting organic monolayers on metal surfaces. To some extent, the molecules exhibit sufficiently strong interaction in their crystalline surroundings. Nevertheless, higher soft X-ray doses as available at undulator beamlines induce chemical reduction even upon short illumination. Therefore, photon-hungry spectroscopic techniques like, *e. g.*, soft X-ray emission spectroscopy require careful control of the beam-induced damage of the investigated substrates.

Acknowledgements

We gratefully acknowledge experimental support by Drs. Th. Schmidt and D. Batchelor (both Universität Würzburg) and Drs. T. Tyliszczak and A. L. D. Kilcoyne (ALS Berkeley). SMM samples were provided by the group of Prof. Dr. R. W. Saalfrank. The project was funded by the DFG within the Sonderforschungsbereich SFB 583 and by the BMBF (contracts 05 KS4WE1 and 05 KS7WE1). We received additional travelling funds from BESSY (BMBF contract 05 ES3XBA/5). We also thank Dr. W. Braun (BESSY) for the fruitful collaboration.

[1] R. W. Saalfrank, H. Maid, A. Scheurer, *Angew. Chem.* **2008**, *120*, 8924 – 8956; *Angew. Chem. Int. Ed.* **2008**, *47*, 8794 – 8824.
[2] G. Aromí, E. K. Brechin, *Struct. Bond.* **2006**, *122*, 1 – 67.
[3] J.-M. Lehn, *Chem. Soc. Rev.* **2007**, *36*, 151 – 160.
[4] G. Mezei, C. M. Zaleski, V. L. Pecoraro, *Chem. Rev.* **2007**, *107*, 4933 – 5003.
[5] D. Gatteschi, *Adv. Mater.* **1994**, *6*, 635 – 645.
[6] G. Christou, D. Gatteschi, D. N. Hendrickson, R. Sessoli, *MRS Bull.* **2000**, *25*, 66 – 71.
[7] R. Sessoli, D. Gatteschi, A. Caneschi, M. A. Novak, *Nature* **1993**, *365*, 141 – 143.
[8] C. Paulsen, J.-G. Park, B. Barbara, R. Sessoli, A. Caneschi, *J. Magn. Magn. Mater.* **1995**, *140 – 144*, 1891 – 1892.
[9] L. Thomas, F. Lionti, R. Ballou, D. Gatteschi, R. Sessoli, B. Barbara, *Nature* **1996**, *383*, 145 – 147.

[10] T. Lis, *Acta Crystallogr.* **1980**, *B36*, 2042 – 2046.
[11] K. Wieghardt, K. Pohl, I. Jibril, G. Huttner, *Angew. Chem.* **1984**, *96*, 66 – 67; *Angew. Chem., Int. Ed. Engl.* **1984**, *23*, 77 – 78.
[12] R. W. Saalfrank, T. Nakajima, N. Mooren, A. Scheurer, H. Maid, F. Hampel, C. Trieflinger, J. Daub, *Eur. J. Inorg. Chem.* **2005**, 1149 – 1153.
[13] R. W. Saalfrank, A. Scheurer, R. Prakash, F. W. Heinemann, T. Nakajima, F. Hampel, R. Leppin, B. Pilawa, H. Rupp, P. Müller, *Inorg. Chem.* **2007**, *46*, 1586 – 1592.
[14] E.-C. Yang, N. Harden, W. Wernsdorfer, L. Zakharov, E. K. Brechin, A. L. Rheingold, G. Christou, D. N. Hendrickson, *Polyhedron* **2003**, *22*, 1857 – 1863.
[15] A. L. Barra, A. Caneschi, A. Cornia, F. Fabrizi de Biani, D. Gatteschi, C. Sangregorio, R. Sessoli, L. Sorace, *J. Am. Chem. Soc.* **1999**, *121*, 5302 – 5310.
[16] R. W. Saalfrank, A. Scheurer, I. Bernt, F. W. Heinemann, A. V. Postnikov, V. Schünemann, A. X. Trautwein, M. S. Alam, H. Rupp, P. Müller, *Dalton Trans.* **2006**, 2865 – 2874.
[17] M. N. Leuenberger, D. Loss, *Nature* **2001**, *410*, 789 – 793.
[18] S. Isaacman, R. Kumar, E. del Barco, A. D. Kent, J. W. Canary, A. Jerschow, *Polyhedron* **2005**, *24*, 2691 – 2694.
[19] B. Cage, S. E. Russek, R. Shoemaker, A. J. Barker, C. Stoldt, V. Ramachandaran, N. S. Dalal, *Polyhedron* **2007**, *26*, 2413 – 2419.
[20] D. Stepanenko, M. Trif, D. Loss, *Inorg. Chim. Acta* **2008**, *361*, 3740 – 3745.
[21] S. Hill, R. S. Edwards, N. Aliaga-Alcalde, G. Christou, *Science* **2003**, *302*, 1015 – 1018.
[22] E. Coronado, A. J. Epsetin, *J. Mater. Chem.* **2009**, *19*, 1661 – 1767 (complete issue).
[23] L. Bogani, W. Wernsdorfer, *Nature Mater.* **2008**, *7*, 179 – 186.
[24] D. Gatteschi, L. Bogani, A. Cornia, M. Mannini, L. Sorace, R. Sessoli, *Solid State Sci.* **2008**, *10*, 1701 – 1709.
[25] D. Gatteschi, R. Sessoli, *Angew. Chem.* **2003**, *115*, 278 – 309; *Angew. Chem. Int. Ed.* **2003**, *42*, 268 – 297.
[26] D. Gatteschi, R. Sessoli, J. Villain, *Molecular Nanomagnets*, Oxford University Press, Oxford, **2006**.
[27] D. N. Hendrickson, G. Christou, H. Ishimoto, J. Yoo, E. K. Brechin, A. Yamaguchi, E. M. Rumberger, S. M. J. Aubin, Z. Sun, G. Aromí, *Mol. Cryst. Liq. Cryst.* **2002**, *376*, 301 – 313.
[28] O. Kahn, *Acc. Chem. Res.* **2000**, *33*, 647 – 657.
[29] K. Petukhov, M. S. Alam, H. Rupp, S. Strömsdörfer, P. Müller, A. Scheurer, R. W. Saalfrank, J. Kortus, A. Postnikov, M. Ruben, L. K. Thompson, J.-M. Lehn, *Coord. Chem. Rev.* **2009**, *253*, 2387 – 2398.
[30] D. W. Boukhvalov, E. Z. Kurmaev, A. Moewes, M. V. Yablonskikh, S. Chiuzbăian, V. R. Galakhov, L. D. Finkelstein, M. Neumann, M. I. Katsnelson, V. V. Dobrovitski, A. L. Lichtenstein, *J. Electron Spectrosc. Relat. Phenom.* **2004**, *137 – 140*, 735 – 739.
[31] U. del Pennino, V. De Renzi, R. Biagi, V. Corradini, L. Zobbi, A. Cornia, D. Gatteschi, F. Bondino, E. Magnano, M. Zangrando, M. Zacchigna, A. Lichtenstein, D. W. Boukhvalov, *Surf. Sci.* **2006**, *600*, 4185 – 4189.
[32] S. Voss, M. Fonin, U. Rüdiger, M. Burgert, U. Groth, Y. S. Dedkov, *Phys. Rev. B* **2007**, *75*, 045102.
[33] S. Voss, M. Fonin, L. Burova, M. Burgert, Y. S. Dedkov, A. B. Preobrajenski, E. Goering, U. Groth, A. R. Kaul, U. Ruediger, *Appl. Phys. A* **2009**, *94*, 491 – 495.
[34] A. F. Takács, M. Neumann, A. V. Postnikov, K. Kuepper, A. Scheurer, S. Sperner, R. W. Saalfrank, K. C. Prince, *J. Chem. Phys.* **2006**, *124*, 044503.
[35] P. Ghigna, A. Campana, A. Lascialfari, A. Caneschi, D. Gatteschi, A. Tagliaferri, F. Borgatti, *Phys. Rev. B* **2001**, *64*, 132413.
[36] R. Moroni, C. Cartier dit Moulin, G. Champion, M.-A. Arrio, P. Sainctavit, M. Verdaguer, D. Gatteschi, *Phys. Rev. B* **2003**, *68*, 064407.
[37] M. Mannini, F. Pineider, P. Sainctavit, L. Joly, A. Fraile-Rodríguez, M.-A. Arrio, C. Cartier dit Moulin, W. Wernsdorfer, A. Cornia, D. Gatteschi, R. Sessoli, *Adv. Mater.* **2009**, *21*, 167 – 171.
[38] M. Mannini, F. Pineider, P. Sainctavit, C. Danieli, E. Otero, C. Sciancalepore, A. M. Talarico, M.-A. Arrio, A. Cornia, D. Gatteschi, R. Sessoli, *Nature Mater.* **2009**, *8*, 194 – 197.
[39] M.-A. Arrio, P. Sainctavit, C. Cartier dit Moulin, C. Brouder, T. Mallah, M. Verdaguer, *J. de Phys. IV: JP* **1997**, *7*, C2-409 – C2-413.
[40] S. Khanra, K. Kuepper, T. Weyhermüller, M. Prinz, M. Raekers, S. Voget, A. V. Postnikov, F. M. F. de Groot, S. J. George, M. Coldea, M. Neumann, P. Chaudhuri, *Inorg. Chem.* **2008**, *47*, 4605 – 4617.
[41] R. W. Saalfrank, I. Bernt, E. Uller, F. Hampel, *Angew. Chem.* **1997**, *109*, 2596 – 2599; *Angew. Chem., Int. Ed. Engl.* **1997**, *36*, 2482 – 2485.
[42] R. W. Saalfrank, I. Bernt, M. M. Chowdhry, F. Hampel, G. B. M. Vaughan, *Chem. Eur. J.* **2001**, *7*, 2765 – 2769.
[43] O. Waldmann, R. Koch, S. Schromm, P. Müller, I. Bernt, R. W. Saalfrank, *Phys. Rev. Lett.* **2002**, *89*, 246401.
[44] H. Bluhm, K. Andersson, T. Araki, K. Benzerara, G. E. Brown, J. J. Dynes, S. Ghosal, M. K. Gilles, H.-C. Hansen, J. C. Hemminger, A. P. Hitchcock, G. Ketteler, A. L. D. Kilcoyne, E. Kneedler, J. R. Lawrence, G. G. Leppard, J. Majzlam, B. S. Mun, S. C. B. Myneni, A. Nilsson, H. Ogasawara, D. F. Ogletree, K. Pecher, M. Salmeron, D. K. Shuh, B. Tonner, T. Tyliszczak, T. Warwick, T. H. Yoon, *J. Electron Spectrosc. Relat. Phenom.* **2006**, *150*, 86 – 104.
[45] F. M. F. de Groot, E. Stavitski, CTM4XAS (version

2.5), Charge Transfer Multiplet Calculations for X-Ray Absorption Spectroscopy, Utrecht University, Utrecht (The Netherlands) **2009**.

[46] B. Toner, S. Fakra, M. Villalobos, T. Warwick, G. Sposito, *Appl. Environ. Microbiol.* **2005**, *71*, 1300 – 1310.

[47] B. D. Yuhas, S. Fakra, M. A. Marcus, P. Yang, *Nano Lett.* **2007**, *7*, 905 – 909.

[48] M. Oku, *J. Electron Spectrosc. Relat. Phenom.* **1994**, *67*, 401 – 407.

[49] D. Collison, C. D. Garner, C. M. McGrath, J. F. W. Mosselmans, E. Pidcock, M. D. Roper, B. G. Searle, J. M. W. Seddon, E. Sinn, N. A. Young, *J. Chem. Soc., Dalton Trans.* **1998**, 4179 – 4186.

[50] D. Collison, C. D. Garner, C. M. McGrath, J. F. W. Mosselmans, M. D. Roper, J. M. W. Seddon, E. Sinn, N. A. Young, *J. Synchrotron Rad.* **1999**, *6*, 585 – 587.

[51] L. Dubois, L. Jacquamet, J. Pécaut, J. Latour, *Chem. Commun.* **2006**, 4521 – 4523.

[52] M. Grabolle, M. Haumann, C. Müller, P. Liebisch, H. Dau, *J. Biol. Chem.* **2006**, *281*, 4580 – 4588.

[53] N. Voevodskaya, F. Lendzian, O. Sanganas, A. Grundmeier, A. Gräslund, M. Haumann, *J. Biol. Chem.* **2009**, *284*, 4555 – 4566.

[54] S. J. George, J. Fu, Y. Guo, O. B. Drury, S. Friedrich, T. Rauchfuss, P. I. Volkers, J. C. Peters, V. Scott, S. D. Brown, C. M. Thomas, S. P. Cramer, *Inorg. Chim. Acta* **2008**, *361*, 1157 – 1165.

[55] S. Bonhommeau, N. Pontius, S. Cobo, L. Salmon, F. M. F. de Groot, G. Molnár, A. Bousseksou, H. A. Dürr, W. Eberhardt, *Phys. Chem. Chem. Phys.* **2008**, *10*, 5882 – 5889.